Laser-induced-resonance calculations for the photodissociation of H_2^+ in an adiabatic electronic-field representation using the radiation-field gauge

S. Manoli and T. T. Nguyen-Dang
Département de Chimie, Faculté des Sciences et de Genie, Université Laval, Québec, Canada G1K 7P4
(Received 3 May 1993)

The properties of the laser-induced first resonance state in the photodissociation of H_2^+ are obtained from calculations in the radiation-field (RF) gauge, also called the velocity gauge, as a function of intensity and wavelength of the field within an adiabatic electronic-field representation, and the results are compared to the corresponding ones obtained using a diabatic RF gauge representation and an adiabatic electric-field gauge representation. Gauge transformation within the coupled equations used for these calculations is also discussed.

PACS number(s): 33.80.Gj, 33.80.Wz, 42.50.Hz, 34.50.Rk

I. INTRODUCTION

Photodissociation of diatomic molecules in intense laser fields has to be investigated using theoretical formalisms that go beyond the traditional perturbative approaches [1–5]. The most effective of such formalisms are the so-called dressed-molecule approach [3,4], which considers the field and the molecule together as a single conservative system, and the Floquet formalism, which considers the time evolution of the molecular system in a classical periodic field [6,7]. Even though both are derived from different considerations, they yield identical coupled equations if the field is intense enough [8,9].

In the dressed-molecule approach, an electronic-field representation can be defined using a basis constructed from the product of field-free electronic states calculated within the Born-Oppenheimer approximation and photon-number states. This electronic-field basis is *diabatic* with respect to radiative interactions because these interactions are included via a nondiagonal *potential* coupling matrix. In the case of H_2^+, if the radiative interactions between nuclear amplitudes of the molecule are expressed as the product of the electric field and the transition dipole moment, i.e., the interaction terms are expressed in the electric field (EF) or length gauge, then not only do the couplings increase with increasing intensity but with increasing internuclear distance as well due to the ionic character of the molecule. Hence a large number of coupled diabatic channels are required to give converged results [8]. Alternatively, the diabatic basis can be transformed so as to diagonalize the potential coupling matrix, and the resulting *adiabatic* channels will be coupled by nonadiabatic interactions of the kinetic type which can be considered negligible at infinite internuclear separations.

In either representation, resonance states are created by the mixing of continuum with bound states. As shown in previous work [9], the calculation of the position and width of adiabatic resonance states at a particular intensity generally requires fewer adiabatic channels than the corresponding calculations of the position and width of diabatic resonance states. In spite of the advantages of the adiabatic representation [9], calculations in this representation are scarce due to the difficulty associated with integrations which properly take into account nonadiabatic couplings.

In the diabatic representation, the calculation of the position and width of the resonance states using the electric-field gauge was done using the complex dilatation method which consists of rotating the nuclear variables into the complex plane, thereby ensuring that the nuclear amplitudes are square integrable in the complex plane [8,10]. The coupled equations can then be solved using a complex-coordinate version of the Numerov algorithm. The imaginary components of the resulting complex eigenvalues correspond to the widths of the resonance states while the real components correspond to their positions. In the adiabatic representation, the coupled equations in the EF gauge have been solved directly using a modified Numerov algorithm, the Nguyen-Dang–Durocher–Atakek (NDDA) algorithm [9,11], which has been specifically derived to take into account nonadiabatic coupling terms. Since the nonadiabatic coupling terms can be neglected at infinite internuclear distances [12], the asymptotic behavior of the adiabatic nuclear amplitudes have been analyzed in terms of a scattering matrix.

In previous work [11], the first resonance state in the adiabatic representation was obtained from EF gauge calculations and it was compared to the one calculated in the diabatic representation also using the EF gauge [8]. It was shown that, in this gauge, diabatic and adiabatic resonance states were not necessarily unitary equivalents. This conclusion was illustrated in part by the existence of *shape* resonances in the adiabatic representation that do not exist in the diabatic representation [11].

It is well known that the choice of gauge representing the matter-field interactions is not unique. Radiative couplings may also be expressed in terms of the product of the vector potential and the momentum operators, the radiation-field (RF) gauge. The best gauge, EF or RF, to use in dynamical calculations has been largely a matter of choice which depends on the system being studied and the intensity of the field, among other criteria. In princi-

ple, the choice of gauge should not matter since they are linked by a unitary transformation. As shown by Reiss [13–15], gauge invariance depends on the approximations, if any, that are used in transforming the Hamiltonian between the EF and RF gauges: approximations such as the long-wavelength approximation (LWA), which, when applied in the center-of-mass reference frame, leads to a dipolar Hamiltonian in the RF gauge but gives rise to a Hamiltonian which has an electric quadrupolar component in the EF gauge. This implies that there is a difference between the LWA and dipole approximations in the EF gauge. Calculation of resonance states in both gauges should give the same results provided the *complete* set of electronic states is included to define the electronic-field basis. In the photodissociation of H_2^+, only the $X\,^2\Sigma_g^+$ and $A\,^2\Sigma_u^+$ electronic states have been used to define the basis. Neglecting the other electronic states is expected to have a small effect on the gauge invariance of the resonances since the other excited states of the H_2^+ molecule are relatively far in energy, and they are not expected to make a large contribution to the resonance calculations. However, recent theoretical investigations of the time-resolved dynamics of the photodissociation of H_2^+ using wave-packet techniques in both the EF and RF gauges give results that do not appear to be gauge invariant [16]. Hence the problem of gauge invariance in photodissociation dynamics does not seem to have been completely resolved. Insofar as the analysis of field-induced resonances calculated in a time-independent Floquet theoretical framework is concerned, the radiative couplings expressed in the RF gauge in both the diabatic and adiabatic representations vanish at large internuclear distances, and hence the asymptotic behavior of the nuclear amplitudes in both representation may be analyzed using unitarily equivalent scattering matrices. Thus the spectrum of resonances in both representations should coincide in this gauge. In contrast, in the EF gauge, the nonadiabatic couplings in the adiabatic representation are negligible at large internuclear distances while, in the diabatic representation, the couplings diverge at infinite internuclear separations. Hence the adiabatic field-induced resonances, located using a scattering matrix approach, do not coincide with the diabatic ones [9].

In this work, the position and width of the field-induced first resonance state in the photodissociation of H_2^+ is calculated in the diabatic and adiabatic representation as a function of intensity and wavelength using the RF gauge, and these results are compared to the corresponding adiabatic EF gauge resonance calculations. Following the developments of Reiss [13–15], the relationship between the EF and RF gauge Hamiltonian will first be examined in the context of high-intensity fields. This review will serve to better identify the conditions under which calculations in both gauges may be compared, in spite of the inevitable use of approximation such as the LWA, the dipole approximation, and the truncation of the electronic Floquet Hamiltonian.

II. THE HAMILTONIAN

The Hamiltonian for a molecule in an electromagnetic field expressed in the RF gauge can be written as

$$\hat{H}(t)=\sum_{\alpha=1}^{N}\frac{1}{2m_\alpha}\left\{\hat{\mathbf{P}}_\alpha-\frac{q_\alpha}{c}\mathbf{A}(\mathbf{r}_\alpha,t)\right\}^2+V(\{\mathbf{r}\})\ , \quad (1)$$

where $\mathbf{A}(\mathbf{r}_\alpha,t)$ is the vector potential, $\hat{\mathbf{P}}_\alpha$ is the kinetic-energy operator, m_α is the mass and q_α is the charge of the αth particle (electron or nucleus), and $V(\{\mathbf{r}\})$ is the potential due to all the charged particles. The vector potential in (1) has been expressed classically because the intensity of the field will be considered to be high [17]. In this case,

$$\mathbf{A}(\mathbf{r}_\alpha,t)=V^{-1/2}\sum_{k,\lambda}\{\boldsymbol{\varepsilon}_{k,\lambda}A_{k,\lambda}(t)\exp(i\mathbf{k}\cdot\mathbf{r}_\alpha)+\text{c.c.}\}\ , \quad (2)$$

where $V^{-1/2}$ is the quantization volume, $\boldsymbol{\varepsilon}_{k,\lambda}$ is the polarization vector of the wave vector k in the field of wavelength λ, and the sum in (2) means that $\mathbf{A}(\mathbf{r}_\alpha,t)$ is the vector potential acting at the point $\mathbf{r}_\alpha$ due to all the modes of the field. The Hamiltonian (1) can be expressed in the EF gauge using the transformation

$$\hat{U}(t)=\exp\left[\frac{i}{\hbar c}\sum_{\alpha=1}^{N}\boldsymbol{\mu}(\mathbf{r}_\alpha)\cdot\mathbf{A}(\mathbf{r}_\alpha,t)\right]\ , \quad (3)$$

where $\boldsymbol{\mu}(\mathbf{r}_\alpha)$ is the dipole operator $q_\alpha\mathbf{r}_\alpha$ of the αth particle in the molecule. Following the developments of Reiss [15], the transformed Hamiltonian

$$\hat{H}'(t)=\hat{U}^\dagger(t)\hat{H}(t)\hat{U}(t)-i\hbar\hat{U}^\dagger(t)\frac{\partial}{\partial t}\hat{U}(t) \quad (4)$$

in the EF gauge can be written as

$$\hat{H}'(t)=\sum_{\alpha=1}^{N}\frac{1}{2m_\alpha}\left\{\hat{\mathbf{P}}_\alpha+\sum_{k,\lambda}\omega_k^{-1}\boldsymbol{\mu}(\mathbf{r}_\alpha)\cdot\mathbf{E}_{k,\lambda}(\mathbf{r}_\alpha,t)\mathbf{k}\right\}^2$$
$$-\sum_{\alpha=1}^{N}\boldsymbol{\mu}(\mathbf{r}_\alpha)\cdot\mathbf{E}(\mathbf{r}_\alpha,t)+V(\{\mathbf{r}\})\ , \quad (5)$$

where $\mathbf{E}_{k,\lambda}(\mathbf{r}_\alpha,t)$ is the electric field of the (k,λ) mode associated with a vector potential through

$$\mathbf{E}_{k,\lambda}(\mathbf{r}_\alpha,t)=-\frac{1}{c}\frac{\partial}{\partial t}\mathbf{A}_{k,\lambda}(\mathbf{r}_\alpha,t) \quad (6)$$

and where the electric field $\mathbf{E}(\mathbf{r}_\alpha,t)$ is defined by

$$\mathbf{E}(\mathbf{r}_\alpha,t)=\sum_{k,\lambda}\mathbf{E}_{k,\lambda}(\mathbf{r}_\alpha,t)\ . \quad (6')$$

In this work, only a single-mode monochromatic field of frequency ω $(=c|\mathbf{k}|)$ will be considered, and hence the summation inside the brackets of (5) as well as the summation of (2) reduce to a single term which is intensity and wavelength dependent.

It is important to note that the LWA has not been imposed on the vector potential in (3); it defines the exact transformation for the derivation of the EF gauge Hamiltonian. To determine the effect of the LWA and dipole approximations, the Hamiltonians (1) and (5) must first be transformed into the center-of-mass (c.m.) coordinate system by defining the position of the c.m. as

$$\mathbf{R}_{\text{c.m.}}=\sum_{\alpha=1}^{N}\frac{m_\alpha}{M}\mathbf{r}_\alpha\ , \quad (7)$$

where M is the total mass of the molecule, and by defining the momentum of the c.m. as

$$\hat{\mathbf{P}}_{\text{c.m.}}=\sum_{\alpha=1}^{N}\hat{\mathbf{P}}_{\alpha}\ . \tag{8}$$

The remaining $(N-1)$-independent relative displacements and momentum operators $\boldsymbol{\rho}_\alpha$ and $\hat{\mathbf{P}}^r_\alpha$, respectively, are given by

$$\boldsymbol{\rho}_\alpha=\mathbf{r}_\alpha-\mathbf{R}_{\text{c.m.}},\quad \alpha=1,2,\ldots,N-1 \tag{9}$$

and

$$\hat{\mathbf{P}}^r_\alpha=\hat{\mathbf{P}}_\alpha-\frac{m_\alpha}{m_N}\hat{\mathbf{P}}_N=\frac{\hbar}{i}\nabla_{\boldsymbol{\rho}_\alpha}=\frac{\hbar}{i}\sum_{\beta}^{N}\left\{\nabla_{\boldsymbol{\rho}_\alpha}\mathbf{r}_\beta\right\}\nabla_{\mathbf{r}_\beta}\ ,$$
$$\alpha=1,2,\ldots,N-1\ . \tag{10}$$

The RF gauge Hamiltonian (1) can now be expressed as

$$\begin{aligned}\hat{H}(t)=&\sum_{\alpha=1}^{N-1}\frac{1}{2m_\alpha}\hat{\mathbf{P}}^{r2}_\alpha+\frac{1}{2M}\hat{\mathbf{P}}^2_{\text{c.m.}}-\frac{1}{2M}\sum_{\alpha,\beta=1}^{N-1}\hat{\mathbf{P}}^r_\alpha\cdot\hat{\mathbf{P}}^r_\beta+V(\{\boldsymbol{\rho}\})-\sum_{\alpha=1}^{N-1}\frac{q_\alpha}{m_\alpha c}\mathbf{A}(\boldsymbol{\rho}_\alpha+R_{\text{c.m.}},t)\cdot\hat{\mathbf{P}}^r_\alpha\\&-\frac{1}{Mc}\sum_{\alpha=1}^{N-1}q_\alpha\mathbf{A}(\boldsymbol{\rho}_\alpha+\mathbf{R}_{\text{c.m.}},t)\cdot\hat{\mathbf{P}}_{\text{c.m.}}+\frac{1}{Mc}\sum_{\alpha,\beta=1}^{N-1}q_\alpha\mathbf{A}(\boldsymbol{\rho}_\alpha+\mathbf{R}_{\text{c.m.}},t)\cdot\hat{\mathbf{P}}_\beta+\sum_{\alpha=1}^{N-1}\frac{q^2_\alpha}{2m_\alpha c^2}\mathbf{A}^2(\boldsymbol{\rho}_\alpha+\mathbf{R}_{\text{c.m.}},t)\\&-\frac{q_N}{Mc}\mathbf{A}\left[\mathbf{R}_{\text{c.m.}}-\sum_{\alpha=1}^{N-1}\frac{m_\alpha}{m_N}\boldsymbol{\rho}_\alpha,t\right]\cdot\hat{\mathbf{P}}_{\text{c.m.}}+\frac{q_N}{Mc}\mathbf{A}\left[\mathbf{R}_{\text{c.m.}}-\sum_{\alpha=1}^{N-1}\frac{m_\alpha}{m_N}\boldsymbol{\rho}_\alpha,t\right]\cdot\sum_{\alpha=1}^{N-1}\hat{\mathbf{P}}_\alpha r\\&+\frac{q^2_N}{2m_N c^2}\left|\mathbf{A}\left[\mathbf{R}_{\text{c.m.}}-\sum_{\alpha=1}^{N-1}\frac{m_\alpha}{m_N}\boldsymbol{\rho}_\alpha,t\right]\right|^2\ .\end{aligned} \tag{11}$$

The LWA assumes that the wavelength of the field is much larger than the dimension of the molecule, and hence $\mathbf{k}\cdot\boldsymbol{\rho}_\alpha$ is much smaller than 1 thereby causing the vector potential to depend only on the position of the c.m. and time. The LWA does *not* imply that $\mathbf{k}\cdot\mathbf{R}_{\text{c.m.}}$ is much less than 1 [13]. In this case, the Hamiltonian (11) becomes

$$\begin{aligned}\hat{H}(t)=&\sum_{\alpha=1}^{N-1}\frac{1}{2m_\alpha}\hat{\mathbf{P}}^{r2}_\alpha+\frac{1}{2M}\hat{\mathbf{P}}^2_{\text{c.m.}}-\frac{1}{2M}\sum_{\alpha,\beta=1}^{N-1}\hat{\mathbf{P}}^r_\alpha\cdot\hat{\mathbf{P}}^r_\beta+V(\{\boldsymbol{\rho}\})-\sum_{\alpha=1}^{N-1}\frac{q_\alpha}{m_\alpha c}\mathbf{A}(\mathbf{R}_{\text{c.m.}},t)\cdot\hat{\mathbf{P}}^r_\alpha-\frac{Q}{Mc}\mathbf{A}(\mathbf{R}_{\text{c.m.}},t)\cdot\hat{\mathbf{P}}_{\text{c.m.}}\\&+\frac{Q}{Mc}\sum_{\alpha=1}^{N-1}\mathbf{A}(\mathbf{R}_{\text{c.m.}},t)\cdot\hat{\mathbf{P}}^r_\alpha+\sum_{\alpha=1}^{N}\frac{q^2_\alpha}{2m_\alpha c^2}|\mathbf{A}(\mathbf{R}_{\text{c.m.}},t)|^2\ ,\end{aligned} \tag{12}$$

where Q is the total charge of the molecule. Applying (12) to H_2^+ using

$$M=2m_p+m_e\cong 2m_p\ , \tag{13a}$$

$$Q=2q_p+q_e=q_p\ , \tag{13b}$$

where m_p and m_e are the masses of the proton and electron, respectively, q_p and q_e are the charges of the proton and electron, respectively, and writing the summations in (12) explicitly in terms of the relative electronic canonical variables

$$\boldsymbol{\rho}_e=\mathbf{r}_e-\mathbf{R}_{\text{c.m.}}\ , \tag{14a}$$

$$\hat{\mathbf{P}}_e=\hat{\mathbf{P}}^r_e \tag{14b}$$

and nuclear canonical variables

$$\boldsymbol{\rho}=\tfrac{1}{2}(\mathbf{r}_1-\mathbf{r}_2)=\tfrac{1}{2}\mathbf{R}\ , \tag{15a}$$

$$\hat{\mathbf{P}}_R=2\hat{\mathbf{P}}^r_p\ , \tag{15b}$$

where $\mathbf{R}$ is the internuclear distance, the Hamiltonian (12) is expressed as

$$\begin{aligned}\hat{H}(t)=&\frac{1}{m_p}\hat{\mathbf{P}}^2_R+\frac{1}{4m_p}\hat{\mathbf{P}}^2_{\text{c.m.}}+\frac{1}{2m_e}\hat{\mathbf{P}}^2_e-\frac{1}{m_p}\hat{\mathbf{P}}_R\cdot\hat{\mathbf{P}}_e+V(\{\mathbf{R},\boldsymbol{\rho}_e\})-\frac{q_p}{m_p c}\mathbf{A}(\mathbf{R}_{\text{c.m.}},t)\cdot\hat{\mathbf{P}}_R-\frac{q_e}{m_e c}\mathbf{A}(\mathbf{R}_{\text{c.m.}},t)\cdot\hat{\mathbf{P}}_e\\&-\frac{q_p}{2m_p c}\mathbf{A}(\mathbf{R}_{\text{c.m.}},t)\cdot\hat{\mathbf{P}}_{\text{c.m.}}+\frac{q^2_e}{2m_e c^2}|\mathbf{A}(\mathbf{R}_{\text{c.m.}},t)|^2+\frac{q^2_p}{2m_p c^2}|\mathbf{A}(\mathbf{R}_{\text{c.m.}},t)|^2\ .\end{aligned} \tag{16}$$

If it is assumed that nuclear and electronic motions are very weakly coupled, then the $\hat{\mathbf{P}}_R\cdot\hat{\mathbf{P}}_e$ term can be neglected relative to the other motions leaving

$$\hat{H}(t)=\frac{1}{m_p}\left\{\hat{\mathbf{P}}_R-\frac{q_p}{2c}\mathbf{A}(\mathbf{R}_{\text{c.m.}},t)\right\}^2+\frac{1}{2m_e}\left\{\hat{\mathbf{P}}_e-\frac{q_e}{c}\mathbf{A}(\mathbf{R}_{\text{c.m.}},t)\right\}^2+\frac{1}{4m_p}\left\{\hat{\mathbf{P}}_{\text{c.m.}}-\frac{q_p}{c}\mathbf{A}(\mathbf{R}_{\text{c.m.}},t)\right\}^2+V(\{\mathbf{R},\boldsymbol{\rho}_e\})\ . \tag{17}$$

The Hamiltonian in the EF gauge (5) can also be transformed into the c.m. frame of reference and, after applying the LWA and the definitions (13) to (15) for H_2^+, becomes

$$\begin{aligned}\hat{H}'(t)=&\frac{1}{m_p}\left\{\hat{\mathbf{P}}_R+\frac{q_p}{2c}\mathbf{R}\cdot\mathbf{E}(\mathbf{R}_{\text{c.m.}},t)\mathbf{k}\right\}^2+\frac{1}{2m_e}\left\{\hat{\mathbf{P}}_e+\frac{q_e}{c}\boldsymbol{\rho}_e\cdot\mathbf{E}(\mathbf{R}_{\text{c.m.}},t)\mathbf{k}\right\}^2\\&+\frac{1}{4m_p}\hat{\mathbf{P}}^2_{\text{c.m.}}+\frac{q_p}{m_p\omega}\mathbf{R}_{\text{c.m.}}\cdot\mathbf{E}(\mathbf{R}_{\text{c.m.}},t)\mathbf{k}\cdot\hat{\mathbf{P}}_R+\frac{q_e^2}{2m_ec^2}\{\mathbf{R}_{\text{c.m.}}\cdot\mathbf{E}(\mathbf{R}_{\text{c.m.}},t)\}^2\\&+\frac{q_e^2}{m_ec^2}\{\boldsymbol{\rho}_e\cdot\mathbf{E}(\mathbf{R}_{\text{c.m.}},t)\}\{\mathbf{R}_{\text{c.m.}}\cdot\mathbf{E}(\mathbf{R}_{\text{c.m.}},t)\}-q_e\boldsymbol{\rho}_e\cdot\mathbf{E}(\mathbf{R}_{\text{c.m.}},t)-q_b\mathbf{R}_{\text{c.m.}}\cdot\mathbf{E}(\mathbf{R}_{\text{c.m.}},t)+V(\{\mathbf{R},\boldsymbol{\rho}_e\})\ ,\end{aligned} \tag{18}$$

where again it has been assumed that the electronic motion is very weakly coupled to the motion of the protons and to the motion of the c.m. and hence the $\hat{\mathbf{P}}_R\cdot\hat{\mathbf{P}}_e$ term has been neglected, as well as the terms which couple the electronic displacement vector to the nuclear momentum operator and the one which couples the c.m. displacement vector to the electronic momentum operator. As discussed by Reiss [13–15], in the RF gauge, the LWA gives the Hamiltonian (17), while, in the EF gauge, the LWA gives the Hamiltonian (18) which contains electric quadrupole and magnetic dipole terms obtained from the $\mathbf{R}\cdot\mathbf{E}(\mathbf{R}_{\text{c.m.}},t)\mathbf{k}\cdot\hat{\mathbf{P}}$ terms [13]. These terms are approximately 200 times smaller than the electric dipole interaction terms for an intensity of 10^{16} W/cm^2 with a wavelength of 100 nm and for an intensity of 10^{14} W/cm^2 with a wavelength of 1000 nm [15]. Hence they can be neglected for field intensities up to $\sim 10^{14}$ W/cm^2, and the Hamiltonian (18) in this dipole approximation will be

$$\begin{aligned}\hat{H}'(t)=&\frac{1}{m_p}\hat{\mathbf{P}}_R^2+\frac{1}{2m_e}\hat{\mathbf{P}}_e^2+\frac{1}{4m_p}\hat{\mathbf{P}}^2_{\text{c.m.}}-q_p\mathbf{R}_{\text{c.m.}}\cdot\mathbf{E}(\mathbf{R}_{\text{c.m.}},t)\\&-q_e\boldsymbol{\rho}_e\cdot\mathbf{E}(\mathbf{R}_{\text{c.m.}},t)+V(\{\mathbf{R},\boldsymbol{\rho}_e\})\ .\end{aligned} \tag{19}$$

A last approximation will be made concerning the motion of the c.m.; it will be assumed that the motion of the c.m. can be adiabatically separated from the motion of the relative internal coordinates of the molecule in both gauges. Therefore, the RF gauge Hamiltonian used in this work is written as

$$\begin{aligned}\hat{H}(t)=&\frac{1}{m_p}\left\{\hat{\mathbf{P}}_R-\frac{q_p}{2c}\mathbf{A}(t)\right\}^2\\&+\frac{1}{2m_e}\left\{\hat{\mathbf{P}}_e-\frac{q_e}{c}\mathbf{A}(t)\right\}^2+V(\{\mathbf{R},\boldsymbol{\rho}_e\})\ ,\end{aligned} \tag{20}$$

while the EF gauge Hamiltonian is written as

$$\hat{H}'(t)=\frac{1}{m_p}\hat{\mathbf{P}}_R^2+\frac{1}{2m_e}\hat{\mathbf{P}}_e^2-q_e\boldsymbol{\rho}_e\cdot\mathbf{E}(t)+V(\{\mathbf{R},\boldsymbol{\rho}_e\})\ , \tag{21}$$

where the field and its associated vector potential now depend only on time. The Hamiltonian (21) has been used in previous calculations on H_2^+ [6,8,9], but its relationship to the corresponding Hamiltonian in the RF gauge (20) has not been fully examined. In going from the EF to the RF gauge Hamiltonian, the matter-field interaction term given by the third term of (21) has simply been replaced by the $\mathbf{A}(t)\cdot\hat{\mathbf{P}}_e$ term of (20) [18]. As seen from (20), this amounts to neglecting the direct interaction between the field and the relative motion of the nuclei. Interestingly, the resulting RF gauge Hamiltonian *is* unitarily equivalent to the EF gauge Hamiltonian (21). This is surprising in light of the approximations and simplifications made in the parallel derivations of both the RF and EF gauge Hamiltonians. These Hamiltonians were obtained using the LWA in the c.m. coordinate system. In the EF gauge, the quadrupolar terms were neglected, thereby highlighting the difference between the LWA and dipole approximations. In both gauges, the correlation between the nuclear and electronic momenta were neglected, and the motion of the c.m. is adiabatically decoupled from the motion of the internal molecular coordinates.

III. THE COUPLED EQUATIONS

In previous work [4–6,8,9], the EF gauge Hamiltonian (21) has been used in the time-dependent Schrödinger equation for the two-channel model of the dissociation of H_2^+ within both the Floquet and electronic-field approaches. These approaches are equivalent at high laser field intensities and hence the Floquet approach will be used in this work. In this approach, the matter-field interaction terms in (20) and (21) can be expressed using classical expressions for the electric field and its associated vector potential as

$$\mathbf{E}(t)=\mathbf{E}_0\cos(\omega t) \tag{22}$$

and

$$\mathbf{A}(t)=-\frac{c}{\omega}\mathbf{E}_0\sin(\omega t)\ , \tag{23}$$

respectively. The solutions of the time-dependent Schrödinger equation

$$i\hbar\frac{\partial}{\partial t}|\Psi_E\rangle=\hat{H}(t)|\Psi_E\rangle \tag{24}$$

are sought for with the Hamiltonian given by (20) or (21). For the photodissociation of H_2^+, the electronic part of the Hamiltonian is written in a truncated basis of the field-free Born-Oppenheimer states defined by

$$\left\{\frac{1}{2m_e}\hat{\mathbf{P}}_e^2+V(\{\mathbf{R},\boldsymbol{\rho}_e\})\right\}\psi_k(\boldsymbol{\rho}_e,\mathbf{R})=E_k(\mathbf{R})\psi_k(\boldsymbol{\rho}_e,\mathbf{R}) , \tag{25}$$

which define the potential energy surfaces $E_k(\mathbf{R})$ that depend parametrically on the nuclear coordinates $\mathbf{R}$. As noted in previous work on H_2^+ [8,9], the nuclear coordinate $\mathbf{R}$ can be replaced by R, and only two solutions of (25) are needed to describe the photodissociation of the ion from the ground state; the $|1\sigma_g\rangle$ and $|1\sigma_u\rangle$ electronic states corresponding to the bound $E_g(R)$ and dissociative $E_u(R)$ potential-energy curves. The periodicity of the applied field and hence of the solution $|\Psi_E\rangle$ can be exploited to express the solution of the full time-dependent Schrödinger equation as a quasienergy state (QES's) defined in terms of a Fourier expansion with respect to the frequency of the applied field ω

$$|\Psi_E,t\rangle=\exp\left\{-\frac{i}{\hbar}Et\right\}\sum_{n=-\infty}^{\infty}\exp(in\omega t)\times[\chi_g^n(R)|1\sigma_g\rangle+\chi_u^n(R)|1\sigma_u\rangle] , \tag{26}$$

where $\chi_g^n(R)$ and $\chi_u^n(R)$ are nuclear amplitudes [6,8]. The QES (26) has been used in the time-dependent Schrödinger equation expressed in terms of the EF gauge Hamiltonian, and, after integration over the electronic coordinates and over one period defined by the frequency of the applied field ω, this gave rise to an infinite set of time-independent coupled equations given by [6,8,9]

$$[\hat{T}_R+E_g(R)+n\hbar\omega-E]\chi_g^n(R)+\tfrac{1}{2}\boldsymbol{\mu}_{gu}(R)\cdot\mathbf{E}_0[\chi_u^{n+1}(R)+\chi_u^{n-1}(R)]=0 , \tag{27a}$$

$$[\hat{T}_R+E_u(R)+(n+1)\hbar\omega-E]\chi_u^{n+1}(R)+\tfrac{1}{2}\boldsymbol{\mu}_{ug}(R)\cdot\mathbf{E}_0[\chi_g^{n+2}(R)+\chi_g^n(R)]=0 , \tag{27b}$$

where $\boldsymbol{\mu}_{jk}(R)$ is the parametrically R-dependent transition dipole moment defined by

$$\boldsymbol{\mu}_{jk}(R)=\int d\boldsymbol{\rho}_e\psi_j^*(\boldsymbol{\rho}_e,R)q_e\boldsymbol{\rho}_e\psi_k(\boldsymbol{\rho}_e,R) . \tag{28}$$

The coupled equations (27) may be written in matrix form [9]

$$[\hat{T}_R-E\underline{I}+\underline{V}_{\mathrm{EF}}^{\mathrm{diab}}(R)]\underline{X}^{\mathrm{diab}}(R)=\underline{0} , \tag{29}$$

where $\underline{I}$ is the identity matrix, and $\underline{V}^{\mathrm{diab}}(R)$ is the diabatic potential matrix

$$\underline{V}_{\mathrm{EF}}^{\mathrm{diab}}(R)=\begin{bmatrix} E_g(R)+(n+2)\hbar\omega & V_{\mathrm{int}}^{\mathrm{EF}}(R) & 0 & 0 & \cdots \\ V_{\mathrm{int}}^{\mathrm{EF}}(R) & E_u(R)+(n+1)\hbar\omega & V_{\mathrm{int}}^{\mathrm{EF}}(R) & 0 & \cdots \\ 0 & V_{\mathrm{int}}^{\mathrm{EF}}(R) & E_g(R)+n\hbar\omega & V_{\mathrm{int}}^{\mathrm{EF}}(R) & \cdots \\ 0 & 0 & V_{\mathrm{int}}^{\mathrm{EF}}(R) & E_u(R)+(n-1)\hbar\omega & \cdots \\ \cdots & \cdots & \cdots & \cdots & \cdots \end{bmatrix} , \tag{30}$$

and $V_{\mathrm{int}}^{\mathrm{EF}}(R)$ is defined by

$$V_{\mathrm{int}}^{\mathrm{EF}}(R)=\tfrac{1}{2}\boldsymbol{\mu}_{ug}(R)\cdot\mathbf{E}_0=\tfrac{1}{2}\boldsymbol{\mu}_{gu}(R)\cdot\mathbf{E}_0 . \tag{31}$$

In (29), $\underline{X}^{\mathrm{diab}}(R)$ is a vector consisting of the diabatic nuclear amplitudes

$$\underline{X}^{\mathrm{diab}}(R)=\begin{bmatrix}\chi_g^{n+2}(R)\\ \chi_u^{n+1}(R)\\ \chi_g^n(R)\\ \chi_u^{n-1}(R)\\ \vdots\end{bmatrix} . \tag{32}$$

In principle, the diabatic potential matrix is of infinite dimension and it is made up of Floquet blocks, each of which consists of an E_g/E_u 2×2 block in (30). An adiabatic electronic-field basis can be defined by diagonalizing $\underline{V}_{\mathrm{EF}}^{\mathrm{diab}}(R)$

$$\underline{V}_{\mathrm{EF}}^{\mathrm{ad}}(R)=\underline{C}^{\dagger}(R)\underline{V}_{\mathrm{EF}}^{\mathrm{diab}}(R)\underline{C}(R) \tag{33}$$

using

$$\underline{X}^{\mathrm{ad}}(R)=\underline{C}^{\dagger}(R)\underline{X}^{\mathrm{diab}}(R) . \tag{34}$$

The resulting adiabatic channels are illustrated in Fig. 1. As in previous work [9], the centrifugal terms obtained from the angular expansion of the nuclear amplitudes have been implicitly included in the diabatic potentials and hence the EF gauge radial adiabatic matrix equation is [9]

$$-\frac{\hbar^2}{m_p}\left\{\frac{d^2}{dR^2}+\underline{Q}(R)\frac{d}{dR}+\underline{W}_{\mathrm{EF}}^{\mathrm{ad}}(R)\right\}\underline{X}^{\mathrm{ad}}(R)=0 , \tag{35}$$

where

$$\underline{Q}(R)=2\underline{C}^{\dagger}(R)\frac{d}{dR}\underline{C}(R) \tag{36}$$

and

$$\underline{W}_{\mathrm{EF}}^{\mathrm{ad}}(R)=\frac{m_p}{\hbar^2}[E\underline{I}-\underline{V}_{\mathrm{EF}}^{\mathrm{ad}}(R)]+\underline{C}^{\dagger}(R)\frac{d^2}{dR^2}\underline{C}(R) . \tag{37}$$

The diabatic coupled equations using the RF gauge Hamiltonian (20) can be derived in a similar manner using either the Floquet or the electronic-field approach. In the RF gauge, the complete interaction Hamiltonian for the H_2^+ molecule

$$\hat{H}_{\rm int}(t)=-\frac{q_p}{m_p c}\mathbf{A}(t)\cdot\hat{\mathbf{P}}_R-\frac{q_e}{m_e c}\mathbf{A}(t)\cdot\hat{\mathbf{P}}_e+\frac{q_e^2}{m_e c^2}|\mathbf{A}(t)|^2 \tag{38}$$

involves terms that couple the field to both the nuclei and the electrons [the fact that m_p is much larger than m_e has been used to neglect the $|\mathbf{A}(t)|^2/m_p$ term]. The electronic momentum operator can be expressed as the commutator

$$\hat{\mathbf{P}}_e=\frac{m_e}{i\hbar}\left[\boldsymbol{\rho}_e,\frac{1}{2m_e}\hat{\mathbf{P}}_e^2+V(\{R,\boldsymbol{\rho}_e\})\right] \tag{39}$$

such that its matrix elements may be expressed as

$$\langle\hat{P}_e\rangle_{jk}=\frac{m_e}{i\hbar q_e}[E_k(R)-E_j(R)]\mu_{jk}(R)\ . \tag{40}$$

Using the expression for the vector potential (23), the coupled equations can be written as

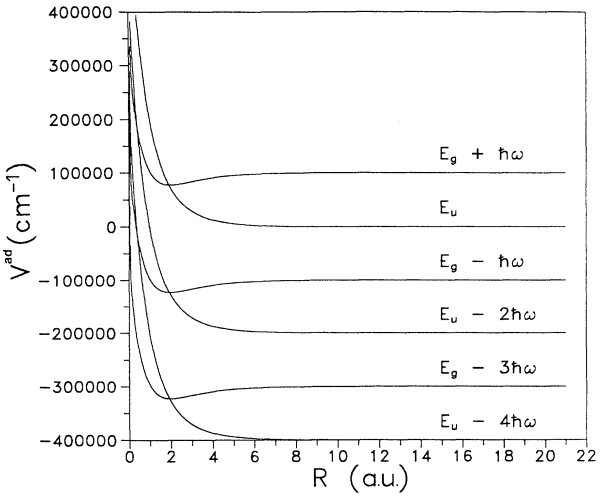

FIG. 1. The adiabatic potential energy curves of H_2^+ in a field of wavelength 100 nm calculated at an intensity of 1.41×10^{13} W/cm^2 obtained from the diagonalization of the EF gauge diabatic potential matrix for a six-channel (three Floquet blocks) matrix equation. The labels on the asymptotes refer to the dresses diabatic potentials used to derive them. The avoided crossings cannot be distinguished on this scale.

$$\left[\hat{T}_R+E_g(R)+n\hbar\omega-E+\frac{q_e^2\mathbf{E}_0^2}{4m_e\omega^2}\right]\chi_g^n(R)-\frac{q_e^2\mathbf{E}_0^2}{8m_e\omega^2}[\chi_g^{n+2}(R)+\chi_g^{n-2}(R)]$$

$$+\frac{[E_u(R)-E_g(R)]}{\hbar\omega}V_{\rm int}^{\rm EF}(R)[\chi_u^{n+1}(R)-\chi_u^{n-2}(R)]+\frac{\hbar q_p}{2m_p\omega}\mathbf{E}_0\cdot\nabla_R[\chi_g^{n+1}(R)-\chi_g^{n-1}(R)]=0\ , \tag{41a}$$

$$\left[\hat{T}_R+E_u(R)+(n+1)\hbar\omega-E+\frac{q_e^2\mathbf{E}_0^2}{4m_e\omega^2}\right]\chi_u^{n+1}(R)-\frac{q_e^2\mathbf{E}_0^2}{8m_e\omega^2}[\chi_u^{n+3}(R)+\chi_u^{n-1}(R)]$$

$$+\frac{[E_g(R)-E_u(R)]}{\hbar\omega}V_{\rm int}^{\rm EF}(R)[\chi_g^{n+2}(R)-\chi_g^n(R)]+\frac{\hbar q_p}{2m_p\omega}\mathbf{E}_0\cdot\nabla_R[\chi_u^{n+2}(R)-\chi_u^n(R)]=0\ . \tag{41b}$$

These coupled equations do not have the same form as those of the EF gauge Floquet picture (27); the second term in (41) arises from the $|\mathbf{A}(t)|^2/m_e$ while the ∇_R term arises from the first term of the interaction Hamiltonian (27), and this term has no equivalent in the EF gauge coupled equations. For simplicity, let

$$V_0=\frac{q_e^2|\mathbf{E}_0|^2}{4m_e\omega^2},\quad \mathbf{V}_p=\frac{\hbar q_p\mathbf{E}_0}{2m_p\omega}\ , \tag{42}$$

and

$$V_{gu}^{\rm RF}(R)=\frac{[E_u(R)-E_g(R)]}{\hbar\omega}V_{\rm int}^{\rm EF}(R)\ . \tag{43}$$

The RF gauge coupled equations (41) may be written in matrix form

$$[\hat{T}_R+\underline{I}\mathbf{V}_p\cdot\nabla_R+E\underline{I}+\underline{V}_{\rm RF}^{\rm diab}(R)+V_0\underline{P}]\underline{X}^{\rm diab}(R)=\underline{0}\ , \tag{44}$$

where $\underline{I}$ is the identity matrix, $\underline{V}_{\rm RF}^{\rm diab}(R)$ is the diabatic potential matrix

$$\underline{V}_{\mathrm{RF}}^{\mathrm{diab}}(R)=\begin{bmatrix} E_g(R)+(n+1)\hbar\omega & -V_{gu}^{\mathrm{RF}}(R) & 0 & V_{gu}^{\mathrm{RF}}(R) & \cdots \\ -V_{gu}^{\mathrm{RF}}(R) & E_u(R)+n\hbar\omega & 0 & 0 & \cdots \\ 0 & 0 & E_g(R)+n\hbar\omega & -V_{\mathrm{gu}}^{\mathrm{RF}}(R) & \cdots \\ V_{gu}^{\mathrm{RF}}(R) & 0 & -V_{gu}^{\mathrm{RF}}(R) & E_u(R)+(n-1)\hbar\omega & \cdots \\ \cdots & \cdots & & \cdots & \cdots \end{bmatrix}, \tag{45}$$

$$\underline{P}=\begin{bmatrix} 1 & 0 & 0 & 0 & -\frac{1}{2} & 0 & 0 & \cdots \\ 0 & 1 & 0 & 0 & 0 & -\frac{1}{2} & 0 & \cdots \\ 0 & 0 & 1 & 0 & 0 & 0 & -\frac{1}{2} & \cdots \\ 0 & 0 & 0 & 1 & 0 & 0 & 0 & \cdots \\ -\frac{1}{2} & 0 & 0 & 0 & 1 & 0 & 0 & \cdots \\ 0 & -\frac{1}{2} & 0 & 0 & 0 & 1 & 0 & \cdots \\ 0 & 0 & -\frac{1}{2} & 0 & 0 & 0 & 1 & \cdots \\ \cdots & \cdots & \cdots & \cdots & \cdots & \cdots & \cdots & \cdots \end{bmatrix}, \tag{46}$$

$$\underline{T}=\begin{bmatrix} 0 & 0 & -1 & 0 & 0 & 0 & 0 & \cdots \\ 0 & 0 & 0 & -1 & 0 & 0 & 0 & \cdots \\ 1 & 0 & 0 & 0 & -1 & 0 & 0 & \cdots \\ 0 & 1 & 0 & 0 & 0 & -1 & 0 & \cdots \\ 0 & 0 & 1 & 0 & 0 & 0 & -1 & \cdots \\ 0 & 0 & 0 & 1 & 0 & 0 & 0 & \cdots \\ 0 & 0 & 0 & 0 & 1 & 0 & 0 & \cdots \\ \cdots & \cdots & \cdots & \cdots & \cdots & \cdots & \cdots & \cdots \end{bmatrix}, \tag{47}$$

and $\underline{X}^{\mathrm{diab}}(R)$ is a vector consisting of the diabatic nuclear amplitudes

$$\underline{X}^{\mathrm{diab}}(R)=\begin{bmatrix} \chi_g^{n+1}(R) \\ \chi_u^{n}(R) \\ \chi_g^{n}(R) \\ \chi_u^{n-1}(R) \\ \chi_g^{n-1}(R) \\ \vdots \end{bmatrix}. \tag{48}$$

Again, these matrices are in principle of infinite dimension.

An adiabatic electronic-field basis can be defined by requiring that the sum of $\underline{V}_{\mathrm{RF}}^{\mathrm{diab}}(R)$ and $V_0\underline{P}$ be diagonalized

$$\underline{V}_{\mathrm{RF}}^{\mathrm{ad}}(R)=\underline{C}^{\dagger}(R)[\underline{V}_{\mathrm{RF}}^{\mathrm{diab}}(R)+V_0\underline{P}]\underline{C}(R) \tag{49}$$

so that the adiabatic nuclear amplitude matrix may be written in the same form as (34). The RF gauge adiabatic channels are illustrated in Fig. 2, and they can be compared to the EF gauge adiabatic channels in Fig. 1. The EF gauge Floquet blocks in Fig. 1 are separated by $2\hbar\omega$, the energy of two photons, while the RF gauge Floquet blocks, designated by both solid and dashed lines in Fig. 2, are separated by the energy of one photon. The configuration of the three RF gauge Floquet blocks in Fig. 2 designated by the solid lines is exactly the same as the configuration of the three EF gauge Floquet blocks in Fig. 1. Hence the solution of a six-channel matrix equation in the EF gauge can be compared to the solution of a ten-channel matrix equation in the RF gauge. As in previous work [9], centrifugal terms obtained from the angular expansion of the nuclear amplitudes have been implicitly included in the diabatic potentials. Hence the radial adiabatic matrix equation to be solved is

$$-\frac{\hbar^2}{m_p}\left\{\frac{d^2}{dR^2}+\left[\underline{Q}(R)-\frac{m_p}{\hbar^2}V_p\underline{C}^{\dagger}(R)\underline{TC}(R)\right]\frac{d}{dR} +\underline{W}_{\mathrm{RF}}^{\mathrm{ad}}(R)-\frac{m_p}{2\hbar^2}V_p\underline{C}^{\dagger}(R)\underline{TC}(R)\underline{Q}(R)\right\} \times\underline{X}^{\mathrm{ad}}(R)=0 , \tag{50}$$

where

$$\underline{W}_{\mathrm{RF}}^{\mathrm{ad}}(R)=\frac{m_p}{\hbar^2}[E\underline{I}-\underline{V}_{\mathrm{RF}}^{\mathrm{ad}}(R)]+\underline{C}^{\dagger}(R)\frac{d^2}{dR^2}\underline{C}(R) \tag{51}$$

and $\mathbf{V}_p$ has been replaced by the scalar V_p. The nonadiabatic coupling matrix $\underline{Q}(R)$ is given by the same expression as the EF gauge nonadiabatic coupling matrix (36).

The EF gauge adiabatic matrix equation (35) and both the diabatic (44) and adiabatic (50) matrix equations contain terms of the kinetic type and hence the use of the generalization of Numerov integration formula of Nguyen-Dang, Durocher, and Atabek [9,11], which has specifically been designed to take into account kinetic coupling terms, is required to solve them.

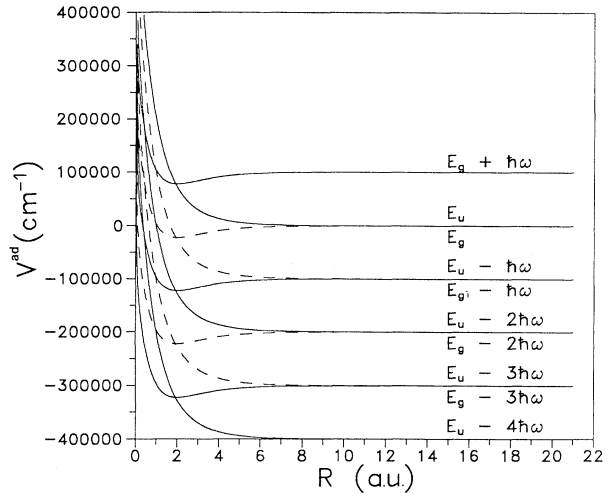

FIG. 2. The adiabatic potential energy curves of H_2^+ in a field of wavelength 100 nm calculated at an intensity of 1.41×10^{13} W/cm^2 obtained from the diagonalization of the RF gauge diabatic potential matrix. This illustration consists of five Floquet blocks and ten dressed channels. The labels on the asymptotes refer to the dressed diabatic potentials used to derive them. The avoided crossings cannot be distinguished on this scale.

In this work, the results of resonance calculations obtained by solving the diabatic and adiabatic RF gauge matrix equations (44) and (50), respectively, will be compared to those obtained by solving the adiabatic EF matrix equation (35).

IV. COMPUTATIONAL ASPECTS

The parametrically R-dependent model potentials for the electronic states involved in the photodissociation of the H_2^+ molecule and the transition dipole moment used in the calculations in this work are the same as those used in previous work [6,8,9]. Other computational considerations such as the evaluation of the elements of the skew-symmetric $\underline{Q}(R)$ matrix and the integration procedure are identical to those described in earlier work in the EF gauge [9]. Integration was carried out to $R=21$ a.u. in all cases, with a step size of 2.5×10^{-3} a.u. Moreover, in the region of avoided crossings of the adiabatic potential curves, this step size was reduced by a factor of 2^n, where n is an integer which depends of the steepness of the nonadiabatic coupling terms [9,11]. The results given in this work have converged with respect to these computational parameters.

Since the couplings in the RF gauge (43) in both the diabatic and adiabatic representations vanish at large internuclear distances, the asymptotic behavior of the nuclear amplitudes can be used to give an energy-dependent S matrix $\underline{S}(E)$ whose determinant can be expressed in terms of an energy-dependent phase

$$\det[\underline{S}(E)]=\exp[2i\delta(E)]\ . \tag{52}$$

The sharp variation of the phase with respect to energy in (52) signals the presence of a resonance. In previous work in the EF gauge [9], in addition to the S matrix obtained from nuclear amplitudes, which are solution of the full adiabatic coupled matrix equation $\underline{S}(E)$, an S matrix $\underline{S}_0(E)$ was also obtained from the asymptotic behavior of adiabatic nuclear amplitudes calculated using *only* the diagonal elements of the adiabatic matrix equation. The $\underline{S}(E)$ was used to identify resonance states resulting from the coupling of bound states to dissociative states, the Feshbach resonances, while $\underline{S}_0(E)$ was used to identify states with finite lifetimes existing on the adiabatic potential energy surfaces, resonances of the type *shape*. However, for the purposes of comparing the diabatic and adiabatic representations, only those resonances arising from the mixing of dissociative and bound electronic states, Feshbach resonances, will be required since there are no *shape* resonances in the diabatic representation. Hence, in this work, the S matrix obtained from the full coupled matrix equations, $\underline{S}(E)$, will be used to identify resonances in all cases.

V. RESULTS AND DISCUSSION

Calculations have been performed with laser wavelengths of 100–200 nm at intensities varying from 10^{10} to $\sim10^{14}$ W/cm^2 to locate the first resonance level. In subsequent results, the position of the first resonance will be expressed in terms of an energy shift $\Delta E=E_r-E_0$ of the position of the resonance E_r from the $v=0$, $J=1$ energy level of the ground electronic state of the H_2^+ molecule at zero intensity E_0.

The solution of the diabatic and adiabatic RF gauge coupled matrix equations (44) and (50), respectively, may be simplified by neglecting the $\underline{TV}_p$ terms in both equations. This has the effect of reducing the number of Floquet blocks required for the calculation from those shown in Fig. 2 to those shown in Fig. 1; the Floquet blocks depicted by dashed lines in Fig. 2 are neglected in this procedure. Calculations using the complete matrix equation have been performed using six channels and they are compared in Table I to the equivalent calculation which used an approximate four-channel matrix equation that did not include the $\underline{TV}_p$ term for a laser wavelength of 100 nm. The results obtained using the approximate coupled equations are not drastically different from those obtained using the complete coupled equations. From Table I, the resonance width calculated in both the diabatic and adiabatic representations is more sensitive to this approximation than the corresponding resonance shift. The diabatic and adiabatic widths obtained from the complete matrix equation differ from the corresponding approximate matrix equation result by at most 1% at low intensities. At high intensities, the differences between the complete and approximate equation results reaches 5%. Results for other wavelengths show similar trends. For both the diabatic and adiabatic representations, the approximate coupled matrix equations represent a reduction in the size of the matrix equation to be solved. Moreover, the solution of the approximate coupled matrix equation can be and was obtained using the traditional Numerov integration scheme. In the case of the diabatic representation, the complete matrix equa-

TABLE I. A comparison of the shift ΔE and width $\Gamma/2$ in cm^{-1} of the first resonance level of H_2^+ in a field of wavelength 100 nm calculated using the complete six-channel coupled RF gauge Hamiltonian matrix equation with those calculated using the equivalent approximate four-channel RF gauge Hamiltonian coupled matrix equation that does not include the $\underline{T}V_p$ term [cf. Eq. (43)] in the diabatic and adiabatic representations. The first column is the $\log_{10}$ of the intensity, the second and third columns are the adiabatic complete and approximate, respectively, coupled equation shift and width, and the fourth and fifth columns are the diabatic complete and approximate, respectively, coupled equation shift and width.

	Adiabatic				Diabatic			
	Complete		Approximate		Complete		Approximate	
$\log_{10}I$	$\Gamma/2$	ΔE	$\Gamma/2$	ΔE	$\Gamma/2$	ΔE	$\Gamma/2$	ΔE
13.15	366.88	266.43	383.18	266.31	399.69	239.75	417.82	239.68
13.00	248.88	191.78	251.26	191.71	265.72	171.88	273.13	171.86
12.75	129.79	109.51	133.16	109.52	142.45	97.15	144.53	97.14
12.50	72.20	62.40	72.97	62.40	78.52	54.69	79.14	54.69
12.25	40.28	35.52	40.52	35.52	43.74	30.76	43.93	30.76
12.00	22.63	20.01	22.64	20.01	24.48	17.30	24.54	17.30
11.75	12.73	11.50	12.68	11.50	13.73	9.73	13.75	9.73
11.50	7.19	6.55	7.12	6.55	7.71	5.47	7.72	5.47

tion must be integrated using the NDDA integration algorithm [11] because the $\underline{T}V_p$ term is a nonadiabatic coupling, denoting a purely nuclear contribution to the radiative interactions. Since this term appears only in the RF gauge coupled equations (41), neglecting it amounts to constructing the RF gauge Hamiltonian using only the electronic-field interactions, i.e., the nuclei-field interactions are neglected. Even though this simplification represents a considerable reduction in computational time owing to the reduction of the dimension of the matrix equation to be solved, it should not be used at intensities much higher than those considered in this work. Henceforth, the results discussed in this work have been calculated using the simplified approximate matrix equation.

Figure 3 shows the first resonance shift ΔE and width $\Gamma/2$ in the adiabatic representation using the RF gauge. The shift and width are divided by the intensity I and plotted against the logarithm of the intensity to facilitate comparisons with previously published EF gauge results [8,9] and to better differentiate between the low- (linear) and high- (nonlinear) intensity regimes. Figures 3(a) and

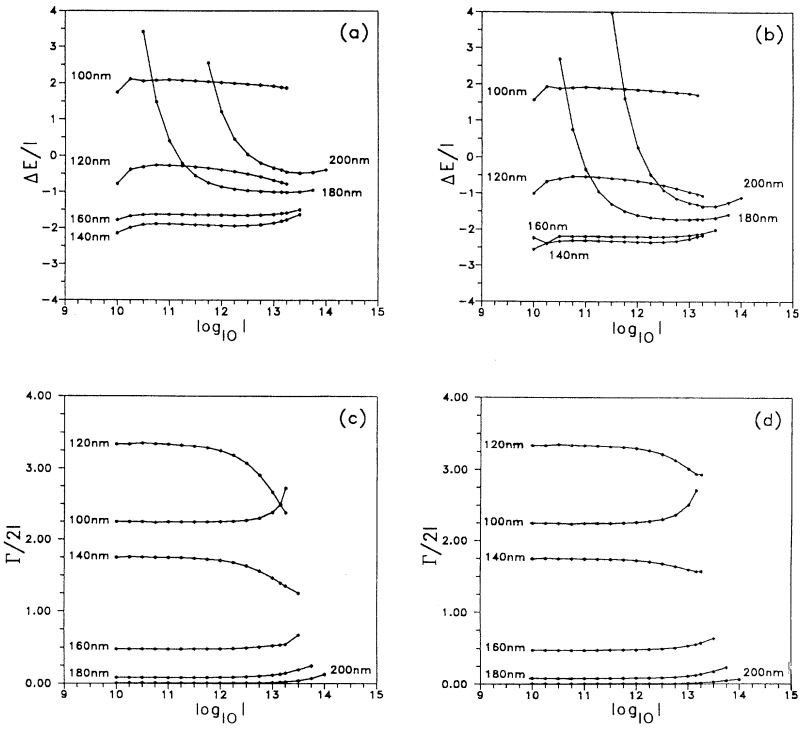

FIG. 3. The variation of the first adiabatic RF gauge resonance shift and width, $\Delta E/I$ and $\Gamma/2I$, respectively (in units of 10^{-11} cm/W), versus $\log_{10}I$ for wavelengths of 100, 120, 140, 160, 180, and 200 nm. These results were calculated using six channels. Panels (a) and (c) give $\Delta E/I$ and $\Gamma/2I$ calculated using five open channels while panels (b) and (d) give $\Delta E/I$ and $\Gamma/2I$ calculated using three open channels.

3(c) depict the resonance shift and width results, respectively, calculated using three coupled Floquet blocks similar to those shown in Fig. 1 with five open channels. These calculations include two Floquet blocks consisting of channels that are dressed by lower photon numbers with respect to the block that supports the position of the resonance state. This means that the resonance state is only accessible by the absorption of photons, in this case absorption of a maximum of five photons, and hence the results of these calculations reflect photon absorption only and no photon emission effects are included. In contrast, Figs. 3(b) and 3(d) depict the corresponding resonance shift and width, respectively, calculated using three coupled Floquet blocks but with three open channels. In these calculations, there is one Floquet block which lies below the one supporting the resonance state which consists of channels dressed by lower photon numbers, the open Floquet block, and another block which lies above the Floquet block supporting the resonance state that consists of channels dressed by higher photon numbers, the closed Floquet block. In this case, the resonance state accounts for absorption of up to three photons from the open Floquet block and emission of up to two photons corresponding to transition to the upper closed Floquet block. Hence the results of such calculations account for photon absorption and emission. The zero-intensity ground-state energy of the $v=0, J=1$ level E_0 used to calculate ΔE was obtained by fitting a few low-intensity points to a straight line since, at low intensities, the shift ΔE is expected to vary linearly with field intensity. In the case of the 180- and 200-nm results in Fig. 3, the nonlinear behavior of the shift at low intensities is due to the presence of a second crossing point, the three-photon crossing point, to the left of the main crossing point, the one-photon crossing point, for example, see Fig. 1, which is low enough in energy to affect the position of the resonance. As discussed in Ref. [9], the nonadiabatic coupling associated with the three-photon crossing point is almost a δ function at these low intensities and hence integration over this crossing point produces large numerical errors in the resonance shift. At lower wavelengths, the three-photon crossing point is high enough in energy so that integration over this region does not contribute any significant errors to the position of the resonance. In the case of the 100-, 120-, 140-, and 160-nm calculations of the low-intensity shift in Figs. 3(a) and 3(b), the nonadiabatic coupling associated with the *main*, i.e., one-photon, crossing point behaves more like a δ function as the field intensity decreases ($\simeq 10^{10}$ W/cm^2 and lower) and the integration yields errors which cause the shift to exhibit a nonlinear behavior with respect to a decrease in intensity. This reflects the well-known fact that the adiabatic representation is more appropriate for strongly coupled diabatic systems than for weakly coupled ones. It is for this reason that the estimate of E_0 was calculated using results ranging from $\log_{10} I \simeq 10.75$ to $\log_{10} \simeq 11.25$ rather than from the lowest-intensity results.

The results of Fig. 3 show the effect of taking into account photon emission in the calculation of the position of the first resonance. The trends in the $\Delta E/I$ curves for all wavelengths in Fig. 3(a) are generally the same as the corresponding ones in Fig. 3(b); however, the absorption-emission results in Fig. 3(b), i.e., those which take into account photon emission as well as absorption (six-channel calculation, three of which are open), are shifted down with respect to the corresponding absorption-only results in Fig. 3(a), i.e., those that only take into account photon absorption (six-channel calculation, five of which are open) by an amount which increases with increasing wavelength and remains constant with intensity. Since the curves in Figs. 3(a) and 3(b) represent $\Delta E/I$, for a given wavelength, the difference between the calculated ΔE of Fig. 3(a) and those of Fig. 3(b) varies linearly with intensity. In principle, the Floquet matrix is of infinite size, and every Floquet block is flanked above by a closed-channel block and below by an open-channel block. Due to the periodicity of the infinite Floquet matrix which, in frequency space, is a consequence of the temporal periodicity of the cw field, the shift and the width of a resonance found within a given Floquet block (a Brillouin zone), henceforth referred to as the reference block, should be independent of the position of this reference block. The resonance state is influenced by the presence of both closed- and open-channel Floquet blocks lying above and below, respectively, the reference block. In practice, a truncation of the Floquet matrix to a finite size introduces a differentiation between the various reference blocks or Brillouin zones. Hence it is not surprising that the properties of resonances supported by frontier blocks, i.e., blocks located at the edge of the truncated Floquet matrix, differ from those of resonances supported by the central or inner zone. The positions and widths of the Floquet resonance states must be determined by calculations which include both open- *and* closed-channel Floquet blocks. Thus the absorption-only shift of Fig. 3(a) reflects the effects of having selected the reference Floquet block to be the uppermost block, i.e., edge effects, while the absorption-emission shift in Fig. 3(b) better reflects the ideal Floquet scheme. This conclusion is reinforced by the results of ten-channel test calculations performed with five open channels which give a shift that is very close to the one obtained using six-channel–three-open calculations for the a wavelength of 100 nm, in the low- to intermediate-intensity regime ($I = 10^{10}$–10^{12} W/cm^2). These results also show that the six-channel calculations are already convergent in this intensity range and residual interblock couplings are indeed weak in the adiabatic representation.

Comparing Figs. 3(c) and 3(d), the horizontal trend of the $\Gamma/2I$ curves for all wavelengths at low intensities is reproduced and, at these low intensities, the results are insensitive to the inclusion of photon emission interactions which is expected since the rotating-wave approximation (RWA) is valid in this intensity regime, and coupling between Floquet blocks can be neglected. Furthermore, in the low-intensity regime, the so-called Markovian regime [19], the resonance width is inversely proportional to the lifetime of the resonance state which, in turn, is inversely proportional to the height of the adiabatic potential barrier at the avoided crossing. As the intensity increases, the height of this barrier decreases and

the lifetime of the resonance state decreases corresponding to an increase in the tunneling rate through the barrier. Hence the resonance width increases with increasing intensity and it is independent of the coupling between Floquet blocks, be they open- or closed-channel blocks. However, at high intensities, the RWA is not valid and coupling between Floquet blocks cannot be neglected and hence the results in Fig. 3(d) differ from those in Fig. 3(c). The observations made from the results of these adiabatic RF gauge calculations have also been made by He, Atabek, and Giusti-Suzor [8] from the results of diabatic EF gauge resonance calculations in the photodissociation of H_2^+. These authors also found that the resonance shift is more sensitive to the presence of open-channel Floquet blocks than the resonance width.

Figures 4 show the shift and width of the first resonance calculated in the diabatic representation using the RF gauge as a function of field intensity and wavelength. As was the case for Fig. 3, Figs. 4(a) and 4(c) give the shift and width resulting from calculations that included three coupled Floquet blocks with five open channels which account for photon absorptions only. Similarly, Figs. 4(c) and 4(d) give the shift and width resulting from calculations which take into account photon absorption and emission by using three coupled Floquet blocks with three open channels. The same technique used to estimate the position of the zero-intensity $v=0, J=1$ energy level from adiabatic RF gauge resonance shift calculations has been used. The E_0 calculated in this way gives a resonance shift that behaves linearly with respect to intensity in low intensity regime.

A comparison of the diabatic RF gauge first resonance shift of Fig. 4 with the adiabatic resonance shift of Fig. 3 shows the absence of any divergent behavior of the diabatic resonance shift at low intensities. The diabatic absorption-emission $\Delta E/I$ curves, Fig. 4(b), show the same trend but are shifted downwards with respect to the corresponding absorption-only curves, Fig. 4(a), as was the case for the adiabatic RF gauge results. The difference between the corresponding absorption-only and absorption-emission $\Delta E/I$ curves increases with increasing wavelength and it is identical to the corresponding difference between the adiabatic $\Delta E/I$ curves discussed previously, Figs. 3(a) and 3(b); this difference is mainly a reflection of the edge effects encountered as a result of truncating the Floquet matrix to a finite size. Finally, the comparison between the pair of Figs. 4(a) and 4(b) with the pair of Figs. 3(a) and 3(b) shows that, as the field intensity increases, the adiabatic resonance shift approaches the corresponding diabatic one.

The behavior of the adiabatic and diabatic absorption-emission RF gauge resonance widths exhibit a common trend, Figs. 3(d) and 4(d). However, the adiabatic $\Gamma/2I$ curves in Fig. 3(d) are shifted downwards with respect to the corresponding diabatic curves in Fig. 4(d) by an amount which decreases with increasing wavelength and which is constant with respect to field intensity. This indicates that, for a given wavelength, the difference between the adiabatic and diabatic results for the resonance width itself $\Gamma/2$ varies linearly with intensity with a slope that decreases with increasing wavelength. The adiabatic and diabatic absorption-only $\Gamma/2I$ curves in Figs. 3(c) and 4(c), respectively, exhibit the same trend, showing the same constant downward shift at low intensities, but they manifest widely differing trends at high intensities. The differences between the diabatic absorption-only and

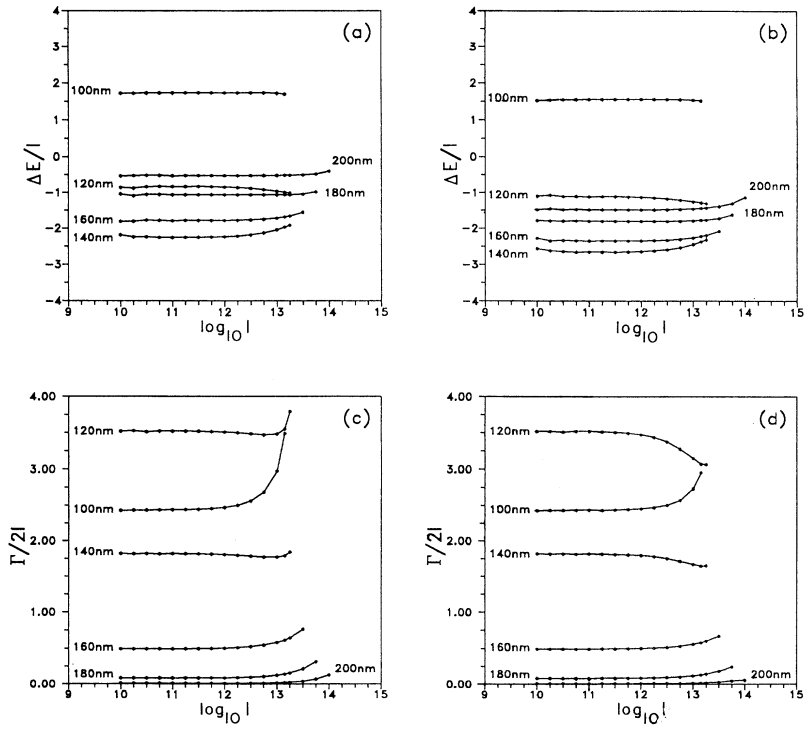

FIG. 4. The variation of the first diabatic RF gauge resonance shift and width, $\Delta E/I$ and $\Gamma/2I$, respectively (in units of 10^{-11} cm/W), versus $\log_{10} I$ for wavelengths of 100, 120, 140, 160, 180, and 200 nm. These results were calculated using six channels. Panels (a) and (c) give $\Delta E/I$ and $\Gamma/2I$ calculated using five open channels while panels (b) and (d) give $\Delta E/I$ and $\Gamma/2I$ calculated using three open channels.

absorption-emission high-intensity $\Gamma/2I$ results, Figs. 4(c) and 4(d), are more significant than the difference between the corresponding adiabatic absorption-only and absorption-emission results, Figs. 3(c) and 3(d), which indicates that, as field intensities increase, absorption-emission effects are more important in the diabatic than in the adiabatic representation. From the numerical viewpoint, this is not surprising since the coupling between different Floquet blocks increases with increasing intensity in the diabatic representation, while, in the adiabatic representation, the nonadiabatic coupling decreases with increasing intensity.

A comparison of Figs. 3 and 4 shows that adiabatic and diabatic results do not coincide even for this first lowest-lying resonance (this can also be seen from the results presented in Table I). Yet, as discussed in Sec. I and Ref. [9], since the RF gauge interchannel couplings vanish at large internuclear distances in both the diabatic and adiabatic representation, the scattering matrices calculated from the asymptotic values of the nuclear amplitudes in both representations were expected to be unitarily equivalent, thereby ensuring that the adiabatic and diabatic resonances would coincide. In this respect, it is interesting to note that while the nonadiabatic coupling between any pair of adiabatic dressed channels is localized and falls to a finite but relatively small value near the origin, the adiabatic (non-diabatic) potential coupling between the corresponding diabatic dressed channels diverges in the vicinity of the origin. This effect is a peculiarity of the RF gauge couplings and it is stronger the higher the field intensity. At this stage, the authors believe that the difference between the adiabatic and diabatic resonances may be due, in part, to the difference between the behavior of the adiabatic couplings in the diabatic representation and the nonadiabatic couplings in the adiabatic representation near the origin. This difference makes it difficult to ensure equivalent boundary conditions near the origin. The photodissociation problem viewed as a half-collision is better defined in the adiabatic representation since the residual nonadiabatic couplings near the origin almost vanish and better justify the use of regular boundary conditions in this limit. The difficulty discussed here, which is essentially associated with the diabatic representation, may be avoided by considering the corresponding full-collision problem which is expected to involve the same resonances as the half-collision problem. This work is currently in progress.

The adiabatic RF gauge results discussed above can be compared to the corresponding adiabatic EF gauge results presented in Fig. 5. The relative trends of the curves describing the adiabatic absorption-emission RF gauge resonance shift and width, Figs. 3(b) and 3(d), are generally the same as the corresponding adiabatic EF gauge results, Figs. 5(b) and 5(d). The effects of photon emission are more noticeable in the trends exhibited by the adiabatic RF gauge resonance shift, as seen by comparing Fig. 3(a) with 3(b), than in the trends exhibited by the adiabatic EF gauge resonance shift, comparing Fig. 5(a) with 5(b). In the low-intensity regime, the adiabatic RF gauge $\Gamma/2I$ curve for a given wavelength in Figs. 3(c) and 3(d) is shifted down with respect to the corresponding EF gauge curve in Figs. 5(c) and 5(d) by an amount which decreases with increasing wavelength. The trends of the corresponding adiabatic RF and EF gauge $\Gamma/2I$ curves differ markedly only in the high-intensity regime. Numerically, this is understood by recalling the funda-

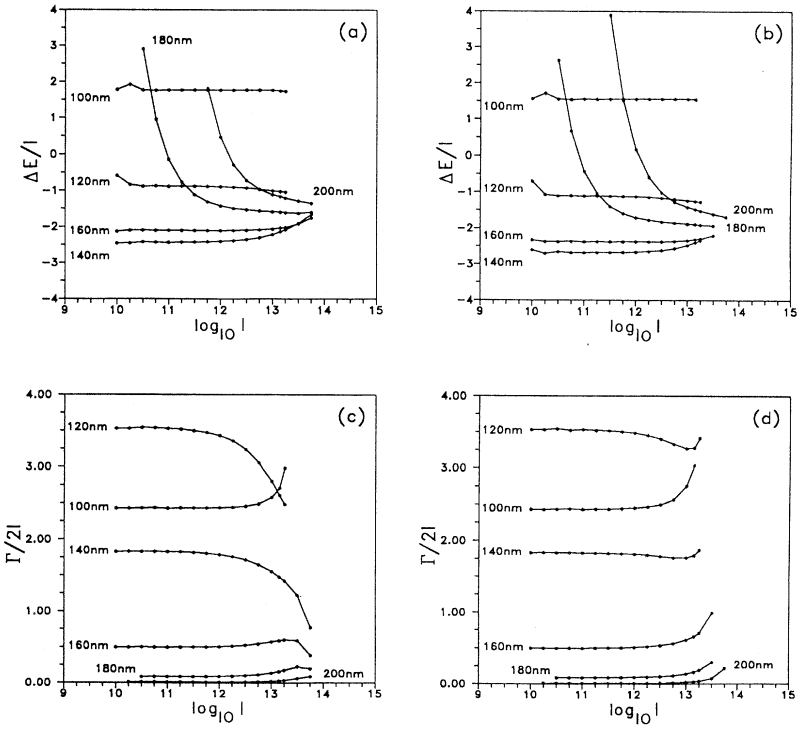

FIG. 5. The variation of the first adiabatic EF gauge resonance shift and width, $\Delta E/I$ and $\Gamma/2I$, respectively (in units of 10^{-11} cm/W), versus $\log_{10}I$ for wavelengths of 100, 120, 140, 160, 180, and 200 nm. These results were calculated using six channels. Panels (a) and (c) give $\Delta E/I$ and $\Gamma/2I$ calculated using five open channels while panels (b) and (d) give $\Delta E/I$ and $\Gamma/2I$ calculated using three open channels.

mentally different asymptotic behavior of the nondiabatic interchannel coupling in the two gauges. The intensity-dependent couplings vanish in the RF gauge, giving rise to completely uncoupled adiabatic potentials that asymptotically perfectly horizontal. In contrast, the EF gauge nondiabatic couplings give rise to asymptotically divergent adiabatic potentials among which small, slowly decaying residual nonadiabatic coupling extend to relatively large internuclear distances. The differences between the EF and RF gauge results, particularly those at lower intensities, cannot be solely attributed to the effects of the different asymptotic behavior of non-diabatic couplings just discussed. Rather, the unitary equivalence which existed between the EF and RF gauge formulation has been intrinsically destroyed by truncation of the problem to the two lowest-lying electronic states of H_2^+. In light of these approximations, the comparison between EF and RF resonance properties appears relatively favorable at low intensities.

Comparing the adiabatic EF gauge results of Fig. 5 with the diabatic results of Fig. 4, it is interesting to note that the low-intensity diabatic RF gauge results, both resonance shift and width, which take into account photon absorption and emission coincide numerically with the corresponding adiabatic EF gauge results.

VI. SUMMARY AND CONCLUSIONS

The diabatic and adiabatic coupled equations which describe the photodissociation of H_2^+ in the RF gauge have been presented. Two versions of each of these matrix equations have been derived, one which includes the explicit nuclei-field coupling terms and another which does not. The EF and RF gauge Hamiltonians, expressed within the LWA and which do not include the effects of the motion of the c.m. were shown to be unitary equivalents provided the EF gauge Hamiltonian was further simplified by neglecting all higher-order multipolar interaction terms. This EF gauge Hamiltonian gives the diabatic and adiabatic coupled equations of Refs. [8] and [9], respectively, used for calculations on the same two-channel system considered here.

The numerical study of the shift and width of the first resonance state in the photodissociation of H_2^+ induced by a laser field of variable frequency and intensity presented in this work leads to the following conclusions.

(i) The presence of the explicit nuclei-field interactions in the RF gauge calculations have little effect on the behavior of the properties of the first resonance state. At field intensities higher than those considered in this work, the presence of these interaction terms may break the unitary equivalence between the LWA RF and EF gauge descriptions.

(ii) The effects of couplings between different Floquet blocks are effectively limited to nearest-neighbor interactions. Specifically, the energy shift of the resonance is more sensitive than the width to an asymmetrical Floquet description of photon absorption and emission.

(iii) The adiabatic resonance calculations are more reliable than the diabatic ones at high-field intensities. In the diabatic EF gauge description, calculations are hindered by asymptotically divergent nondiabatic couplings arising because of the ionic character of the molecule while, in the diabatic RF gauge description, calculations are hindered by divergent radiative couplings near the origin. In contrast, in the adiabatic representation, the nonadiabatic couplings are localized near the avoided crossings of the adiabatic potential energy curves and hence there are no ambiguous boundary conditions either at the origin or as R approaches infinity. However, as the field intensity decreases, the nonadiabatic couplings near the avoided crossings behave more like δ functions and they cause large numerical integration errors in the results.

The expected coincidence between the adiabatic EF and RF gauge resonances due to the previously discussed unitary equivalence of the EF and RF gauge simplified Hamiltonians was not observed, although the comparison between the adiabatic EF and RF results did reveal qualitative similarities in these behavior of the properties of first resonance state with respect to field intensity and wavelength. This lack of invariance is mainly due to the truncation of the electronic Hamiltonian to a two-state representation.

ACKNOWLEDGMENTS

We wish to thank Professor O. Atabek (Orsay, France) for stimulating discussions. The financial support of the Natural Sciences and Engineering Research Council of Canada (NSERCC) is gratefully acknowledged. This work was also partially supported by the Network of Centers of Excellence Programme in association with NSERCC through the Center of Excellence for Molecular and Interfacial Dynamics.

[1] N. M. Kroll and K. M. Watson, Phys. Rev. A **13**, 1018 (1976).
[2] A. M. F. Lau and C. K. Rhodes, Phys. Rev. A **16**, 2392 (1977); A. M. F. Lau, *ibid.* **13**, 139 (1976).
[3] T. F. George, J. Phys. Chem. **86**, 10 (1982); T. F. George, I. H. Zimmerman, J.-M. Yuan, J. R. Laing, and P. L. DeVries, Acc. Chem. Res. **10**, 449 (1977).
[4] T. T. Nguyen-Dang and A. D. Bandrauk, J. Chem. Phys. **80**, 4926 (1984); **79**, 3256 (1983).
[5] A. D. Bandrauk and O. Atabek, in *Lasers, Molecules and Methods,* edited by J. O. Hirshfelder, R. E. Wyatt, and R. D. Coalson (Wiley, New York, 1989), Vol. LXXIII, p. 283.
[6] S.-I. Chu, J. Chem. Phys. **75**, 2251 (1981).
[7] J. Shirley, Phys. Rev. **138**, B979 (1965).
[8] X. He, O. Atabek, and A. Giusti-Suzor, Phys. Rev. A **38**, 5586 (1988).
[9] T. T. Nguyen-Dang and S. Manoli, Phys. Rev. A **44**, 5841 (1991).
[10] W. P. Reinhardt, Annu. Rev. Phys. Chem. **33**, 223 (1982).
[11] T. T. Nguyen-Dang, S. Durocher, and O. Atabek, Chem. Phys. **129**, 451 (1989).
[12] T. T. Nguyen-Dang, S. Manoli, and R. Chaudhury (un-

published).
[13] H. R. Reiss, Phys. Rev. A **29**, 698 (1984).
[14] H. R. Reiss, Phys. Rev. A **22**, 770 (1980).
[15] H. R. Reiss, Phys. Rev. A **19**, 1140 (1979).
[16] H. Abou-Rachid, T. T. Nguyen-Dang, R. K. Chaudhury, and X. He, J. Chem. Phys. **97**, 5497 (1992).
[17] M. H. Mittleman, *Introduction to the Theory of Laser-Atom Interactions* (Plenum, New York, 1980).
[18] A. Giusti-Suzor, X. He, O. Atabek, and F. H. Mies, Phys. Rev. Lett. **64**, 515 (1990); X. He, O. Atabek, and A. Giusti-Suzor, Phys. Rev. A **42**, 1585 (1990).
[19] R. D. Gilbert and R. N. Porter, J. Chem. Phys. **89**, 3057 (1988).